Prospects for the cavity-assisted laser cooling of molecules

Benjamin L. Lev,[1,*] András Vukics,[2,3] Eric R. Hudson,[1,†] Brian C. Sawyer,[1] Peter Domokos,[3] Helmut Ritsch,[2] and Jun Ye[1]

[1]*JILA, National Institute of Standards and Technology and the University of Colorado Department of Physics,*
University of Colorado, Boulder, Colorado 80309-0440, USA
[2]*Institut für Theoretische Physik, Universität Innsbruck, Technikerstrasse 25, A-6020 Innsbruck, Austria*
[3]*Research Institute for Solid State Physics and Optics, P. O. Box 49, H-1525 Budapest, Hungary*
(Received 25 May 2007; published 4 February 2008)

Cooling of molecules via free-space dissipative scattering of photons is thought not to be practicable due to the inherently large number of Raman loss channels available to molecules and the prohibitive expense of building multiple-repumping laser systems. The use of an optical cavity to enhance coherent Rayleigh scattering into a decaying cavity mode has been suggested as a potential method to mitigate Raman loss, thereby enabling the laser cooling of molecules to ultracold temperatures. We discuss the possibility of cavity-assisted laser cooling of particles without closed transitions, identify conditions necessary to achieve efficient cooling, and suggest solutions given experimental constraints. Specifically, it is shown that cooperativities much greater than unity are required for cooling without loss, and that this could be achieved via the superradiant scattering associated with intracavity self-localization of the molecules. Particular emphasis is given to the polar hydroxyl radical (OH), cold samples of which are readily obtained from Stark deceleration.

PACS number(s): 37.10.Vz, 37.20.+j, 37.10.De

I. INTRODUCTION

The experimental realization of large samples of ultracold, ground-state dipolar molecules would be a major breakthrough for research in fields as diverse as ultracold collisions and chemistry to quantum-information processing and the study of novel correlated states of matter [1]. In particular, the anisotropic dipole-dipole interaction becomes non-negligible for polar clouds below approximately 100 μK. Exotic states of dipolar matter, such as field-linked states and dipolar crystals, may be observable in this regime [2]. If the rich field of ultracold alkali-metal Feshbach physics is any measure, then ultracold molecular collisions and chemistry in the presence of the dipolar interaction and external electrical or magnetic fields promises to be fascinating [3–5]. Moreover, the precision motional control attainable only at ultralow temperatures is crucial for constructing the architectures necessary to realize quantum logic gates or spin-lattice simulations using the dipolar interactions [6,7].

While many techniques for ultracold, ground-state polar molecule production show promise, none so far have simultaneously yielded the low temperatures and high densities required to pursue these goals. Photoassociation of ultracold atoms and subsequent optical pumping to the molecular ground state [8,9] have achieved lower sample temperatures ($\sim$100 μK) than techniques such as buffer gas cooling ($\sim$400 mK) [10]. The Stark decelerator provides a nice compromise between density and temperature [11,12] and produces samples in their rovibronic ground state. Electric and magnetic trapping of samples as cold as 10 mK at densities greater than 10^6 cm^{-3} have been demonstrated [13,14].

However, new cooling techniques are required if we hope to push well below the 1 mK regime.

Unlike atoms, molecules typically have a large number of channels into which a given excited state can decay. This makes the efficient free-space laser cooling [15] of molecules challenging due to practical limits on the number of lasers one can build and operate to achieve ground-state repumping after each photon scattering event [16] (for a practical scheme involving only several repumpers, see Ref. [17]). Evaporative and sympathetic cooling techniques are quite promising, but require an initial density higher than what is currently available and is sensitive to the particular molecular species' collision cross section, which is generally unknown [18]. Cavity-assisted laser cooling [19,20] is a promising—though not fully understood—solution in that it provides dissipative cooling largely independent of the details of the molecular structure.

The purpose of this paper is to elaborate on an important distinction between the cavity cooling of atoms versus that of molecules: for efficient cooling, molecules must be strongly coupled to the cavity mode while for atoms weak coupling is sufficient. This difference has important consequences for the practical experimental realization of molecular cavity cooling and should be considered in addition to the issues raised in Refs. [19–22].

Section II analyzes the cavity cooling system as it pertains to molecules, and Appendix A provides analytical details regarding the molecular cavity QED system. This is followed in Secs. III–V by a discussion of techniques to enhance molecule-cavity coupling given realistic constraints on cavity geometry and quality. Feasibility given molecular sample densities and temperatures is assessed in Sec. VI. For concreteness, we focus our attention on Stark deceleration of the OH radical, a highly polarizable molecule well suited for exploring dipolar physics [2,23], cold collisions [5,24], precision measurements of fundamental constants [25,26], and quantum-information processing [6,26].

---

*Present address: Department of Physics, University of Illinois at Urbana-Champaign, Urbana, IL 61801, USA. benlev@uiuc.edu

†Present address: Department of Physics, Yale University, New Haven, CT 06520, USA.
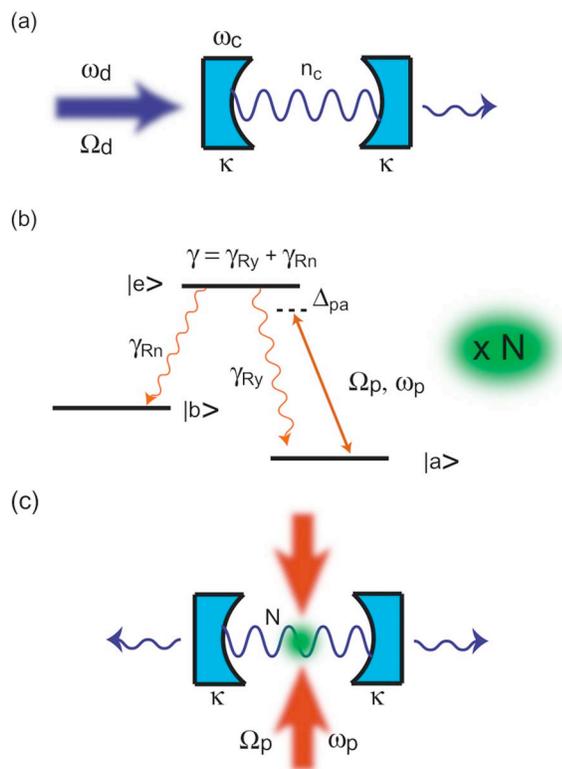
FIG. 1. (Color online) (a) Fabry-Pérot cavity with resonance frequency ω_c driven by a laser of frequency ω_d and drive strength Ω_d, defined in Eq. (A3). In steady state, there are $n_c = \langle a^\dagger a \rangle$ intracavity photons which escape the cavity via the mirrors at the rate 2κ. (b) Three-level representation of the N intracavity molecules. A classical laser field of Rabi frequency Ω_p and frequency ω_p couples the ground state $|a\rangle$ to the electronically excited state $|e\rangle$, whose frequency difference is ω_a. Excitations decay at the total rate γ. Assuming $|e\rangle$ is unsaturated, population is elastically (Rayleigh) scattered back to $|a\rangle$ at the rate γ_{Ry}. Population is lost to the myriad molecular states, represented collectively by $|b\rangle$, at the Raman scattering rate γ_{Rn}. The difference between ω_a and the transition frequency ω_b between $|b\rangle$ and e is much larger than Δ_{pa}. (c) The molecule-cavity system may be pumped by the cavity drive laser, a transverse pump beam (shown), or both. The transverse pump beam of frequency ω_p and Rabi frequency Ω_p is typically red detuned from both the cavity and the molecular resonance ($\omega_p < \omega_c \ll \omega_a$). The N molecules may be trapped or transiently passing through the cavity mode.

II. CAVITY COOLING OF MOLECULES VERSUS CLOSED-TRANSITION ATOMS

Cavity-assisted laser cooling of molecules brings together many otherwise disparate disciplines: cavity quantum electrodynamics (QED), molecular physics, and laser cooling and trapping. The cavity cooling system—as it pertains to molecules—is illustrated in Fig. 1, in which a standing wave cavity is combined with a three-level system. From a semiclassical viewpoint, the molecules act as a nonlinear element that coherently transfers excitation from the red-detuned transverse pump field to the higher-frequency (bluer) intracavity field. Because the blue-detuned field leaks out of the cavity stochastically, energy proportional to the fields' frequency difference is extracted from the system at a rate proportional to the cavity linewidth 2κ. Consequently, the molecules' motion is cooled, as this is the only mechanism from which to extract this energy difference.

While cavity cooling was originally discussed in the context of cooling via driving the cavity mode [19,27], we will focus on pumping via transverse beams, which provides strong cooling in all three dimensions [28,29]. Figure 1(c) depicts the configuration for three-dimensional (3D) transverse pumping, though the two pump beams in the plane perpendicular to the page are not shown. Throughout this paper, unless otherwise stated, discussion is confined to the transverse pumping scenario.

Because two-level atoms naturally possess a closed transition—i.e., one in which the atom relaxes back to the original ground state after each scattering event—such an atom may be efficiently cooled using free-space Doppler cooling (see Ref. [15] for more details). The red-detuned lasers are nearly resonant with the atomic transition, producing strong cooling forces while incoherently scattering from the atom. At larger detunings, the character of the scattering process becomes coherent in nature, and cooling ceases due to the lack of a dissipation channel. However, if the atom is placed inside an optical resonator, a new dissipation channel becomes available to the system; namely, the stochastic leakage of intracavity photons through the cavity mirrors. As long as the cooling lasers are red detuned from the cavity resonance, cooling of the atom is again possible no matter how far the cavity and cooling laser are detuned from the atomic transition. Only the rate at which cooling occurs is reduced by the large detuning. Upon each scattering event, the atom always relaxes to its ground state and is ready to scatter again: The atom is slightly heated due to photon recoil if the photon is scattered into free space, but the atom is cooled if the photon is scattered into the cavity mode.

The ratio between the rate of scattering into the cavity mode, Γ_c, versus the free-space scattering rate Γ_a is known as the cooperativity:

$$C = \frac{\Gamma_c}{\Gamma_a} = \frac{g^2}{\kappa \gamma},\tag{1}$$

where g is the atom-cavity coupling rate, 2κ is the cavity decay rate, and $1/\gamma$ is the excited-state lifetime of the atom. When $C \gg 1$ (and $g \gg [\kappa, \gamma/2]$), the system is in the strong-coupling regime [30,31], and the coherent atom-cavity dynamics dominate over the dissipative rates κ and γ. A small cooperativity ($C < 1$) decreases the efficiency of the cooling process since the cooling rate is proportional to C and the final temperature limit is $T_f \propto \kappa(1 + C^{-1})$ [28]. Cooling is still possible in the weak-coupling limit, albeit less optimally. Such cooling for two-level systems has been experimentally achieved in both limits [32–34] and studied in detail theoretically [20,29,35–37].

Molecular structure fundamentally alters and complicates this picture for two-level atom-cavity cooling. After scattering a photon into free space, the molecule can relax back to the multitude of metastable molecular states—spin orbit, rotational, and vibrational—via inelastic Raman scattering.

Figure 1(b) depicts a three-level atom representing a molecule in which all the metastable states are bundled into state $|b\rangle$. Upon excitation from the pump field Ω_p, the molecule can relax by either Rayleigh scattering back to the ground state $|a\rangle$ at the rate γ_{Ry} or Raman scattering to $|b\rangle$ at the rate γ_{Rn}. The sum of γ_{Ry} and γ_{Rn} is constrained to total the linewidth of the excited state $|e\rangle$. The generally low free-space branching ratio $\Upsilon = \gamma_{Ry}/\gamma_{Rn}$ results in population shelving after only a few photon scattering events, thereby prematurely quenching the cooling process. The only solution for preventing population shelving—given the impracticalities of building numerous repumpers—is to ensure that there is a vanishingly small probability that the molecule will Raman scatter during the cooling time.

This branching ratio is fixed by the molecular structure and it cannot be modified by detuning except when using detunings that are incredibly large $\Delta_{pa} \approx \omega_b$ [38]. In other words, even though the molecule is unsaturated and coherently scatters the pump field, there remains a fixed—and generally large—probability for Raman loss per Rayleigh scattering event, regardless of how large the detuning. While Υ cannot be modified by reasonably large detuning, the rate of scattering into the cavity, and thus the cooling rate, can be made to be larger than the Raman scattering rate by a factor equal to $(1+\Upsilon)C$. The ratio Υ is for most molecules no larger than approximately unity (see Appendix B for the case of OH). Therefore, the rate of scattering into the cavity versus Raman loss is approximately equal to the cooperativity C. This point has been overlooked in all previous treatments of molecular cavity cooling, resulting in an overoptimistic assessment of the efficacy of this technique for efficiently producing ultracold molecular samples.

For atoms such as cesium, only one additional laser is required to repump the atom back to its ground state, where the cooling laser, associated with the pump field Ω_p can continue the cooling process. While building several repumpers becomes prohibitively complex and expensive, one may use a very-far-off resonance transverse pump laser to simultaneously address all higher-lying metastable states, as was described recently in Ref. [22]. However, doing so naturally decreases the cooling rate by the ratio Ω_p^2/Δ_{pa}^2 as described by Eq. (A16). This low cooling rate in the far-detuned case makes practical implementation difficult because of the short interaction time between hot molecules and the small cavity mode volume. Cavities useful for cooling large samples occupy too small a solid angle for appreciable Raman suppression, but one can attempt to compensate a small single-mode cooperativity by using a multimode cavity, as explored in Sec. III and Refs. [22,28].

A more sophisticated treatment of the cooling rate—whose derivation we omit here but which is applicable in both the strong- and weak-coupling regimes (see Ref. [39])—confirms the role of cooperativity as a benchmark for whether or not the particle can cool before loss occurs. The ratio of the average velocity damping rate β to the free-space scattering rate is

$$\frac{\beta}{\gamma\langle\hat{\sigma}_+\hat{\sigma}_-\rangle} = \frac{2\omega_{\rm rec}}{\gamma}\frac{{\rm Im}[(D^*)^2(z_c^2 - g^2)]}{|D|^2|z_c|^2},\qquad(2)$$

where $z_c \equiv -\kappa + i\Delta_{pc}$, $z_a \equiv -\gamma + i\Delta_{pa}$, and $D \equiv z_c z_a + g^2$. The pump-cavity (Δ_{pc}) and pump-molecule (Δ_{pa}) detunings are

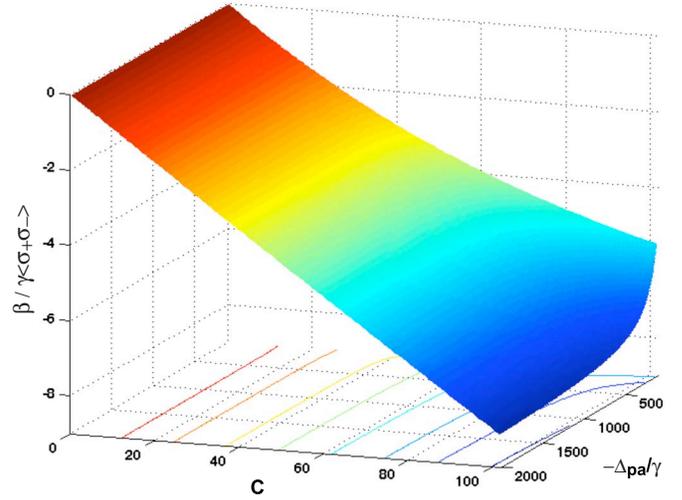
FIG. 2. (Color online) Ratio of the cooling rate to the spontaneous emission rate, $\beta/(\gamma\langle\hat{\sigma}_+\hat{\sigma}_-\rangle)$, in which a negative-valued ratio indicates cooling. Parameters chosen for an OH molecule electronically excited in the cavity described near the end of Sec. III which has a finesse of 5000 and length of 2 cm. The detuning Δ_{pc} is set such that the pump field is $-\kappa$ detuned from the lower dressed state.

depicted in Figs. 1 and 5. Figure 2 plots this ratio versus the cooperativity and the detuning from the molecular resonance. The equations for the ratio of cooling to spontaneous emission in the cavity pumping case (i.e., $\Omega_d \neq 0$ and $\Omega_p = 0$) are cumbersome and are not listed here. In both cases, the ratio is less than unity when $C \leq 1$, as expected. This holds true for cooling to the blue of the cavity resonance as well.

Unlike for two-level atoms, here the magnitude of the cooperativity is central to the fundamental question of how the cavity cooling of molecules can still be effective given that Raman loss is not quenched via the far detuning of the cooling lasers as previously thought. Our conclusion is that molecular cavity cooling is achievable as long as four conditions are met. (1) The collective cooperativity of the intracavity molecular sample must be greater than unity. This is to ensure that photons are scattered into the cavity mode much more frequently than into free space. (2) The linewidth of the cavity resonance should be narrow enough so that the bandwidth of the light scattered into the cavity mode is much less than the frequency separation between the ground state and the metastable states. (3) No cavity mode accidently coincides in frequency with a Raman transition to a metastable state (though see Ref. [22], wherein this is used to cool the molecule's internal degrees of freedom when an initially ground-state molecular sample is unavailable).

These conditions ensure that the cooling rate is faster than the Raman transition rate since photons are preferentially scattered into the cavity, which can only admit light capable of inducing Rayleigh and not Raman transitions. The second condition is easy to achieve experimentally since most cavities of interest possess linewidths smaller than a few tens of megahertz while metastable rotational and vibrational levels are typically more than several gigahertz above the rovibronic ground state. Similarly, the third condition is readily met by fine-tuning the molecule-cavity detuning because

both the molecular metastable states and the cavity modes are relatively sparse and the bandwidth of high cavity finesse is limited. Experimental difficulty lies in satisfying the first condition, as achieving strong coupling is challenging even for ultracold, easily trapped atomic systems [31]. An additional fourth condition must be met for the realistic cavity cooling of molecules: (4) The molecules must spend enough time in the cavity mode volume to reach their cooling limit, but not long enough to Raman scatter. Satisfying this last condition is experientially difficult given the high temperatures and low densities of current ground-state molecular samples.

In Appendix A, we derive the expression for cooperativity by solving the joint molecule-cavity quantum master equation. This is done in the detuning limits appropriate for understanding the cavity cooling of molecules in both the weak- and strong-coupling regimes. We now turn to techniques we propose and review for achieving effective strong coupling for realistic experimental scenarios.

III. ENHANCING SINGLE-MOLECULE COOPERATIVITIES WITH MULTIMODE CAVITIES

A standard method used to achieve larger cooperativities is to decrease the volume of the cavity while simultaneously increasing its finesse. This is the route taken by single-atom cavity QED research [30,31], but it is not suitable here as one wants to cool large diffuse samples several millimeters in width that would not fit into the required submillimeter-sized cavities. Moreover, to maintain a high g^2/κ ratio, one needs to increase the finesse to the 10^4 or 10^5 regime. Unfortunately, the strongest molecular electric dipole transitions (in light molecules like OH) are typically in the blue to uv wavelengths, and cavity finesses much greater than 10^3 are currently commercially unavailable in the near uv.

The geometry of the cavity is primarily constrained by the molecular beam size or trapped cloud dimension and by the lack of high-finesse mirrors in the uv. Moreover, there is a trade-off between cooling volume and g: a large cavity waist provides a large cooling volume, but g will be correspondingly smaller. In the case of OH produced by a Stark decelerator, the cavity length must be at least ≥ 5 mm to ensure that most of the molecules are enveloped by the mirrors, but ≤ 20 cm for practical assembly. For OH excited on the $P_1(1)$ transition (see Appendix B), $C=10^{-1}$ for the TEM$_{00}$ mode of a cavity of radius of curvature R and length L approximately equal to 2 cm and finesse $F=5000$. This cooperativity is certainly not sufficient for ensuring that the cooling rate will dominate the Raman loss rate.

One may wonder whether cooling on purely vibrational transitions is more feasible given the high-finesse coatings available in the infrared and the relatively small number of repumping lasers required to close the transition. Unfortunately, the low decay rate of the vibrational transitions mitigates their utility for realistic cooling in all but long-lifetime traps (see Sec. VI). For instance, OH's first vibrational transition at $\lambda = 2.8$ μm, which naturally has the largest Υ—equal to 1.6—has a slow, $\gamma = 2\pi \times 2.7$ Hz, decay rate [40]. With a single-mode $R \approx L = 1$ cm, $F = 10^5$ cavity, the

cooperativity is $C = 34$, and the best achievable rate of scattering into the cavity would be $C\gamma = 2\pi \times 100$ Hz. The first vibrational overtone, at 1.4 μm, possesses a lifetime roughly a factor of 2 smaller, but has a wavelength at which it is much easier to obtain high-power lasers. A similar cavity would give $C = 17$ and a maximum scattering rate into the cavity of $2\pi \times 23$ Hz. However, in both cases the cavity waist is only ~ 60 μm, which decreases the time fast molecules would spend in the cavity mode.

Before examining how multimode cavities can help increase C for electronic transitions, we note that increasing the single-particle cooperativity by "seeding," i.e., driving the cavity with a nonzero Ω_d, does not help to stimulate more photon exchange from the pump beam to the cavity mode. The same number of photons would be stimulated back from the cavity to the pump beam, thereby canceling the energy loss and adding recoil heating and molecular saturation.

Given these restrictions on minimum cavity length and maximum finesse, another method for increasing single-molecule cooperativity is to increase the number of cavity modes available. One could do this by wrapping more cavities around the molecule, but this is highly impractical. Near-degenerate cavities—such as confocal, near-planar, and concentric cavities—offer an ideal solution [28] in that they can support many modes within the cavity linewidth κ. The molecule can now scatter blueshifted photons into many modes, effectively increasing g by a large multiplicative factor n_{eff}.

Vuletić *et al.* [28] and others previously [41] have shown that confocal cavities provide a better compromise between cooling rate and cooling volume over the other cavities (though the concentric has superior cooling rate performance [28]). Consequently, we will focus solely on the confocal cavity geometry. For this geometry, $\kappa = \pi c/2RF$, where the length and radius of curvature are equal, $L = R$, and the cavity waist is simply $w_0 = \sqrt{R/k}$ [42]. Realistic cavity mirrors have spherical aberration which limits the gains otherwise achievable with a confocal cavity. Nevertheless, as long as $F < kR$, using a confocal cavity does increase the cooperativity over the single-mode case. In the uv, with the largest finesse one could hope to obtain, $F \approx 5000$, the cavity length must be less than 1 mm for a single-mode cavity to be optimal, which is too small for accommodating the diffuse molecular cloud.

The cooperativity of a single-mode cavity, $C = 2F\Delta\Omega/\pi = 6F/\pi kL$, can be enhanced to the following value, which is limited by spherical aberration (SA) (assuming a dipole scatterer oriented perpendicular to the cavity axis):

$$C_{\text{SA}} = 3F\Delta\Omega_{\text{SA}}/4\pi^2 = 3\sqrt{2F/\pi kR}. \tag{3}$$

The following ratio provides an estimate of the effective number of additional modes:

$$n_{\text{eff}} = \sqrt{\frac{C_{\text{SA}}}{C}} = \left(\frac{\pi kR}{2F}\right)^{1/4}. \tag{4}$$

The solid angle of the confocal cavity—which is still much less than unity for cavities of interest—may be related to that of a single-mode cavity of equal length and F by

$$\Delta\Omega_{SA} = 8n_{eff}\Delta\Omega/3. \tag{5}$$

For $F=5000$, $R=10$ cm, and $\lambda=308$ nm—parameters suitable for the first electronic transition in OH—the effective enhancement is $n_{eff}=5$. As a concise figure of merit, one would like to have a confocal cavity that simultaneously maximizes spherical-aberration-limited cooperativity and the cooling area near the cavity waist, $A \approx \pi w_0^2$. The product is

$$C_{SA}A = \sqrt{\frac{18FR}{\pi k^3}}. \tag{6}$$

We see from this expression that the optimal mirror quality and geometry is sensitive only to the product of F and R, and a longer confocal cavity is favorable for fixed finesse. This expression is not entirely fair, however, because a confocal cavity's mode volume is not limited by the TEM$_{00}$ waist w_0, but rather by the convolved waists of all the accessible modes. For a spherically aberrated confocal cavity, this waist is $w_{SA}=2R_{SA}=2(2\pi R^3/kF)^{1/4}$ [28], whose ratio to w_0 is

$$\frac{w_{SA}}{w_0} = 2(kR/F)^{1/4}. \tag{7}$$

This is always greater than unity for useful confocal cavities.

In addition, these figures of merit do not factor in cooling time, proportional to κ [see Eq. (A16)], which is important for a transient molecular sample. We will discuss this consideration more in Sec. VI. Wavelength is not generally a tunable parameter, but redder transitions are favorable. For the $P_1(1)$ OH transition listed in Appendix B, an $L=R=2$ cm, $F=5000$ cavity gives $[C_{SA},\kappa,g_0,w_0,w_{SA}]=[1.1,2\pi\times(7.5\times10^5 \text{ Hz}),2\pi \times(9.0\times10^4 \text{ Hz}),30 \ \mu\text{m},0.3 \text{ mm}]$. Using the confocal cavity, a factor of $\sim$12 has been gained versus the single-mode case (for which $C=0.09$), but even with the aid of a confocal cavity, one still cannot achieve a cooperativity much greater than unity for cavities accommodating samples of OH. For an $R=L=10$ cm cavity, which would be better for molecular sample insertion and which also may be easier to obtain at a finesse as high as $F=5000$ in the uv, the cavity parameters become $[C_{SA},\kappa,g_0,w_0,w_{SA}]=[0.47,2\pi\times(1.5 \times10^5 \text{ Hz}),2\pi\times(1.8\times10^4 \text{ Hz}),70 \ \mu\text{m},1 \text{ mm}]$.

In practice, this C_{SA} is most likely an upper bound. In the experiments of Vuletić *et al.* [32,33,43], the cavity happened to be misaligned from perfect confocality by $\sim$20 μm in the plane perpendicular to the cavity axis. This splits the degeneracy of the cavity modes over a bandwidth of 200 MHz from the TEM$_{00}$ mode position. Consequently, for their $R=7.5$ cm, $F=2000$ near-confocal cavity at 852 nm, n_{eff} should have equaled $\sim$4.5, but was experimentally found to be between 2.7 and 3.2, or 60%–70% of the expected value at the frequency of maximum mode density [43]. If we take this reduction as a pessimistic bound, then one can expect a cooperativity of $C_{SA}\approx[0.73,0.31]$ for the OH cavity cooling systems of cavity length 2 and 10 cm, respectively. The mode volume was 200 times larger than that of the TEM$_{00}$ mode [43], which is 95% of what Eq. (7) would predict for an ideal, spherically aberrated confocal cavity.

The multimode enhancement n_{eff} may be more accurately calculated by taking into account the actual confocal mode structure, as noted in Ref. [29]. This is done analytically using modes that are effectively uniform over the cavity length and by employing a numerical calculation that includes the Gouy-phase term. This results in the following expression for n_{eff}:

$$n_{eff} = \frac{(2M' + 1)!!}{(2M')!!}, \tag{8}$$

where $2M'$ is the maximum mode index, $M=(M'+1)^2$ are the total number of modes seen by the scatterer, and !! is the double factorial. Until the paraxial approximation breaks down for very large M, i.e., when $M\lambda\gg L$, n_{eff} grows roughly linearly with mode number as we expect from the previous discussion. The number of modes supported by the cavity of Vuletić *et al.* [43] was measured to be 220, which produces $n_{eff}=4.3$ from using Eq. (8). This is consistent with Eq. (4)'s value of 4.5, and the experimental near-confocal cavity realizes $\sim$70% of this enhancement. For predictions of future cavity performance, Eq. (4) seems to be sufficient.

Using the numerical confocal cavity calculations, the authors of Ref. [29] reveal a constructive intracavity mode interference effect that reduces the temperature limit $\hbar\kappa/k_B$ by as much as 20% for scatterers offset from the cavity midpoint. The cooling rate could be increased as well, though this effect would need to be confirmed with future simulations. While multimode cavities can aid in increasing cooperativity, we must conclude from the above estimations that, even with an optimally designed cavity, experimentally realistic confocal cavities cannot push C much beyond unity.

IV. COMPLICATIONS AND BENEFITS OF MULTI-INTRACAVITY SCATTERERS

As we have seen in the previous sections, efficient molecular cavity cooling is not possible when $C<1$, as is the case for the $P_1(1)$ transition of OH when the cavity is made long enough to accommodate an experimentally realizable sample. The Raman loss rate will dominate the cooling rate, prematurely quenching the cooling process. For multiple intracavity molecules, cooling is still impossible as long as the molecules act independently of one another and Γ_c is unmodified by many-particle effects. In other words, because the Rayleigh-to-Raman scattering ratio Υ will never be much larger than unity with no repumpers (or even with a single one), the $C>1$ regime is necessary to enhance coherent Rayleigh scattering into the cavity mode over the Raman free-space scattering. To achieve this strong coupling in the absence of collective effects, one has no other recourse but to make small cavities, an impractical compromise if one intends to cool large samples.

The situation of multiple intracavity scatterers adds many-body complexity to the cooling physics, but also a means to increase the per molecule cooperativity beyond unity. To understand how this collective enhancement may arise, let us first consider N randomly spaced scatterers inside a cavity, as depicted in Fig. 3. For simplicity, we assume all N molecules
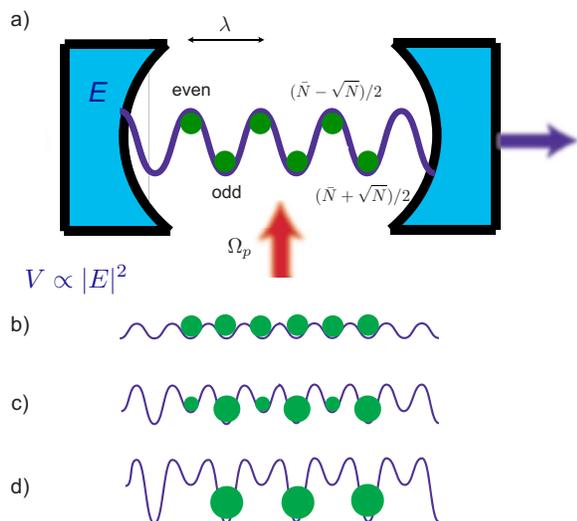
FIG. 3. (Color online) (a) Cartoon of multiple intracavity particle scattering and self-localization. Green dots represent the scatterers and the blue sinusoidal line is the intracavity field E. There are two antinodes per wavelength, distinguished by opposite even or odd phases. The even are represented as the upper antinodes while the odd are the lower. (b) Below a threshold transverse pump Rabi frequency $\Omega_p < \Omega_{th}$, the molecules at the even and odd sites experience an identical dipole trapping force, proportional to $|E|^2$. The random nature of the molecule position implies that at any given time there could be $\sqrt{N}$ more molecules in the odd sites than the even. (c) This leads to an increase in scattered light from the unpaired odd molecules, and the interference with the pump beam creates an ever deeper optical potential for molecules in the odd sites. (d) The even sites are depopulated over the odd, leading to a phase transition from particles located at every antinode to a λ spacing. Concomitantly, superradiance ensues, which increases the per molecule cooperativity by N. The choice of odd over even is arbitrary and the symmetry is spontaneously broken in favor of one versus the other.

are located at the antinodes. Molecules at the nodes do not couple to the field ($\psi = 0$) and those offset from both the node and antinodes have a diminished coupling ($\psi < 1$). We can renormalize N to $N_{eff} = \Sigma_i^N \psi_i$ and consider the N_{eff} molecules equally distributed among the antinodes (we will drop the "eff" subscript from this point forward). There are two antinodes per wavelength and the electric field oscillates exactly π out of phase between them. We designate every other antinode as "even" or "odd" to highlight this phase difference. Figure 3 depicts the even and odd antinodes, along with the (on average) $\bar{N}/2$ molecules in the even sites and $\bar{N}/2$ in the odd. In the absence of motional fluctuations, there are exactly the same number of molecules at the two types of antinodes. For every even molecule that scatters a photon in the cavity mode from the pump beam, there will be another odd molecule that scatters a $\lambda/2$-displaced photon along the cavity axis. These two photons destructively interfere, preventing cavity field buildup.

The molecules have a finite temperature, however, and statistical fluctuations will cause momentary imbalances in the particle number at the even versus odd sites. Assuming Poissonian fluctuations about the mean, at any given moment

there are $(\bar{N} + \sqrt{N})/2$ molecules in the odd sites versus $(\bar{N} - \sqrt{N})/2$ in the even. Of course, the choice of excess molecules in the odd sites is arbitrary, but we will assume this for concreteness. These additional $\sqrt{N}$ molecules in the odd sites are unpaired by any molecules located at integer multiples of $\lambda/2$ and therefore scatter photons into the cavity without destructive interference. Thus, a cavity field is built up with Rabi frequency proportional to $\sqrt{N}g$. This produces a per molecule cooperativity equal to

$$C = \frac{1}{N} \frac{(\sqrt{N}g)^2}{\kappa \gamma} = \frac{g^2}{\kappa \gamma}, \tag{9}$$

which is equal to the single-particle cooperativity.

No multiparticle cooperative effect is seen in the cavity scattering rate—which is $N\Gamma_c$—even though the spectrum of the joint molecule-cavity system exhibits an eigenmode splitting proportional to $\sqrt{N}g$. This highlights the difference between pumping the cavity mode itself (Ω_d) versus pumping the molecular mode directly with a beam transverse to the cavity axis (Ω_p). In the latter case, the molecules act as independent scatterers when the rate at which photons are coupled to and then leaked from the cavity mode is observed. In the former, the molecules interact with the intracavity field in phase and collectively act as a giant dipole that modifies the cavity transfer function (molecule-cavity spectrum).

The situation is dramatically modified if the pump is made stronger than a critical field $\Omega_p \gtrsim \Omega_{th}$ [44,45]. Because the cavity field is red detuned from the molecular resonance, an optical dipole trap may be formed with trap minima centered at the cavity antinodes. However, an intracavity field will not be formed if there is no population imbalance between even and odd sites. As the particle positions fluctuate, a population imbalance will form and a cavity field will be generated. If this thermal position fluctuation is weaker than the ensuing optical dipole trap, then the imbalance between even and odd wells will grow in a runaway (positive feedback) process: Eventually all the molecules will migrate to favored set of wells as this further increases the cavity field and the trap depth. A lattice of periodicity λ will form in every other antinode of the intracavity dipole trap whose strength is proportional to $|E|^2$ (see Fig. 3 and Ref. [33]). Since scattered pump photons into the cavity mode now *constructively* interfere, a large cavity field is built up proportional to Ng. The resulting collective single-particle cooperativity is now

$$C = \frac{1}{N} \frac{(Ng)^2}{\kappa \gamma} = \frac{Ng^2}{\kappa \gamma}, \tag{10}$$

which is N times the single-particle cooperativity $C_N = NC$. The total cavity emission is now superradiant, $N^2 \Gamma_c$ [46,47], and the per particle scattering rate into the cavity mode is collectively enhanced to $N\Gamma_c$. Since one can place many molecules inside the cavity mode, the collective cooperativity can be much greater than unity, $C_N \gg 1$. Raman scattering can now be completely suppressed relative to the elastic scattering rate. Note that these dynamics constitute a spontaneous symmetry-breaking phase transition—initial fluctuations

determine whether the particles localize at the even or odd sites.

V. THRESHOLD FOR SUPERRADIANCE

Satisfying the conditions for triggering this phase transition from a random particle distribution to one of self-organization is of crucial importance to achieving molecular cavity cooling. We now address the criteria for reaching threshold Ω_p^{th} by exploring what is known about this phenomenon and applying it to the task of cooling molecules. The threshold condition has been derived in two ways [45]. The first method employs a mean-field approximation that assumes an intracavity gas of constant density, which is valid in the thermodynamic limit $N \to \infty$, $g \to 0$, $\kappa = \text{const}$, and $Ng^2 \propto N/V = \text{const}$. For driving the lower dressed state below resonance by an amount equal to κ, i.e., $\Delta_{pc} = NU - \kappa$, where NU is the energy shift of the $|-\rangle$ dressed state in the presence of N molecules (see Appendix A and Ref. [44]), the threshold is

$$\Omega_p \geq \Omega_p^{\text{th}} = \sqrt{\frac{k_B T}{\hbar \kappa}} \frac{\kappa |\Delta_{pa}|}{\sqrt{N}g} \sqrt{2}. \qquad (11)$$

We see that the depth of the optical dipole trap at threshold scales linearly with temperature ($V_{\text{th}} \propto \Omega_{\text{th}}^2$), scales inversely with the temperature limit $T_f \approx \hbar \kappa / k_B$, and is inversely proportional to the rate at which pump photons are scattered into the cavity mode, $\propto Ng^2/\kappa \Delta_{pa}^2$. This may be simply understood from the statement that the trap depth must be large enough to quench the diffusion due to thermal energy.

A threshold that scales inversely with $\sqrt{N}$ would not necessarily prevent the triggering of self-localization in experimentally realizable samples of molecules, but numerical calculations [45] indicate that a hysteresis effect in the phase transition pushes the onset out to larger pump fields. The numerically verified threshold becomes

$$\Omega_p \geq \Omega_{\text{th}} = \sqrt{\frac{k_B T}{\hbar \kappa}} \frac{\kappa |\Delta_{pa}|}{N^{1/4} g} \frac{\sqrt{\pi}}{2}. \qquad (12)$$

This scaling of the molecule number as $N^{-1/4}$ instead of $N^{-1/2}$ could make the triggering of superradiance quite difficult to achieve experimentally.

A major impediment to triggering threshold is the need to do so without saturating the transition. In other words, one cannot simply increase Ω_p without a cost in the number of spontaneous Raman emissions. While Ω_p must be greater than threshold,

$$\Omega_p > \sqrt{\frac{k_B T}{\hbar \kappa}} \frac{\kappa |\Delta_{pa}|}{N^{1/x} g}, \qquad (13)$$

where x might equal 2 or 4, the saturation condition must additionally be satisfied:

$$s \approx \frac{\Omega_p^2}{4\Delta_{pa}^2} \ll 1. \qquad (14)$$

This implies that the molecule number must be much greater than

$$N_0 > \left(\sqrt{\frac{k_B T}{\hbar \kappa}} \frac{\kappa}{2g\sqrt{s}} \right)^x. \qquad (15)$$

Using the following parameters for OH in the 2 cm confocal cavity described in Sec. III and assuming T=10 mK, we have $N_0 > 8.5 \times 10^3$ for $x=2$ and $N_0 > 7.3 \times 10^7$ for $x=4$. As discussed in Sec. VI, N_0 could be achievable for $x=2$ with improvements in Stark deceleration, but not likely achievable for $x=4$. Thus, the question of whether the threshold scales as $N^{-1/2}$ or as $N^{-1/4}$ is of paramount importance.

Seeding the cavity by driving the cavity mode itself with $\Omega_d \neq 0$ is one possible method to increase the effectiveness of the transverse cavity cooling scheme, and the phase of the drive field with respect to the pump field has been previously shown to affect the symmetry breaking of the self-localization process [39]. Seeding introduces an intracavity optical dipole trap without having to first scatter from the intracavity molecular medium. One might expect this to hasten the cooling process or decrease the number of molecules required for threshold, but neither effect has thus far been seen in quantum Monte Carlo simulations. This may be due to the fact that a lattice formed by driving the cavity does not contribute to the positive feedback mechanism responsible for self-localization. Nevertheless, any possible method for reducing the threshold requirements for localization warrants more investigation via additional numerical simulations.

Reference [48] identified a mechanism that suppresses free-space scattering well over what is expected from the C_N factor, once self-localization has been triggered. This is due to pump-cavity mode interference in which the collective molecular dipole oscillates out of phase with respect to the pump, suppressing the molecules' excitation. This effect points to another method for achieving superradiance in the case where $N < N_0$: increase the saturation s as the molecules enter the cavity to lower the criteria for reaching threshold. Once self-localization is established, spontaneous emission should be quenched, and the process only sacrifices a fraction of the initial molecules to achieve self-localization for the remaining ones. For example, this technique may be employed for cooling on the vibrational transitions which would nominally require $N_0 > 10^7$ for $x=2$, but can only Raman scatter at a maximum rate $\gamma/2 \approx 2\pi \times 50$ Hz.

The simulations in Ref. [45] suggest that the threshold should scale with particle number as $x=4$, but the experimental results on self-localization [33,43,49] are consistent with $x=2$. References [43,49] attribute this experimental $x=2$ scaling to the onset of recoil-induced resonances (RIRs) [50], but it is noted in Ref. [44] that RIRs would lead only to transient enhancements as opposed to the long-lived collective states described by self-localization. Future work will elucidate the dynamics of this phase transition with additional simulations. Questions to be explored are how the transition threshold scales with intracavity particle number; the role of seeding; the characteristic onset time for superradiance; and how many molecules are lost before spontaneous emission is suppressed in the self-localized state. An additional scenario for simulations to explore is the case in which the recoil energy of the particle of interest, $\hbar \omega_{\text{rec}}$, is comparable to the final cooling temperature $\hbar \kappa / k_B$. All these ques-

tions are of crucial interest for understanding the efficacy of using transversely pumped cavities to cool molecules. This latter question is of particular interest for the relatively light OH molecule whose recoil energy 12 μK is comparable to $\hbar\kappa/k_B = 7$ μK for the 10 cm confocal cavity described above. In the next section we discuss experimental considerations for the cooling of molecules, and, in particular, OH.

VI. EXPERIMENTAL CONSIDERATIONS

Most of the physics to be studied with polar molecules requires them to be in their rovibronic ground state. Supersonic expansions of the molecules entrained in a buffer gas produce packets of polar molecules with quenched rotational and vibrational motion. The technique of Stark deceleration [11] can readily produce slow packets of these ground-state molecules, and in particular, the polar molecule OH [12]. OH is produced via either water discharge or photolysis of nitric acid. When entrained in Xe or Kr, nearly all of the OH—upon expansion—is in the lowest rovibrational $^2\Pi_{3/2}$ Λ-doublet ground states. Although the packet that is formed has a much narrower velocity spread than expected from a Maxwell-Boltzmann distribution, the mean center-of-mass (c.m.) velocity is approximately 400 m/s when Xe is used as the buffer gas. The packet has a $\sim$15% velocity spread in the longitudinal direction, but only a $\sim$7% velocity spread in the transverse dimensions. Thus, in the moving frame, the molecular packet is cold (on the order of 1 K). Before slowing the packet to near-zero c.m. velocity, the packet must pass through a skimmer to prevent backscattering from collapsing the supersonic expansion and to limit the flux of unwanted gas into the decelerator chamber.

A major practical difficulty with cavity-assisted laser cooling of molecules involves ensuring that a sufficiently large molecular sample experiences the mode volume of the cavity for a long enough period of time to cool. At best, cavity waists are no larger than a millimeter, and ground-state polar molecules have yet to be produced in sufficient number at c.m. velocities below $\sim$10 m/s. For the technique of Stark deceleration, Fig. 4 shows the inherent trade-off between slowed packet density and final velocity.

The efficiency curve is divided into four zones, each zone being amenable to a different regime of cavity cooling. Postskimmer, the OH packet is typically of density 10^8–10^9 cm^{-3}, as shown in zone I in Fig. 4. Because the packet is moving at high velocity, it experiences the cavity mode for only a short time. However, the number of OH in the cavity mode may be sufficiently large to trigger rapid cooling. Self-localization happens no faster than $1/\kappa$, but seems to occur within tens of microseconds or less [33,45]. It may be possible to transversely cool the fast OH packet with a cavity. Since Stark deceleration would be much more efficient with an OH packet of narrower transverse velocity spread [52], the cooling in zone I could lead to the Stark slowing of many more molecules in zones II–IV.

Zones II and III offer a compromise between particle number and cavity transit time. In zone II, it may be possible to increase the molecule-cavity interaction time by redirecting the molecule along the cavity axis with an electrostatic
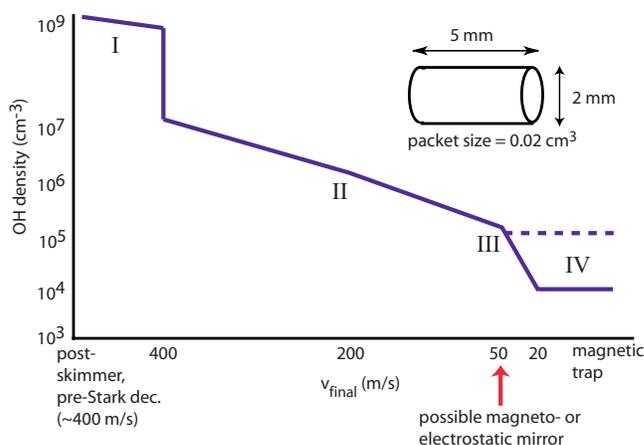

FIG. 4. (Color online) Approximate experimental OH Stark-decelerator efficiency curve—density versus final velocity—for the JILA apparatus [14,51,52]. Inset shows the approximate volume of the OH packet in zones II and III. The packet is larger in the pre-Stark-decelerator zone I, and expands to fill the magnetic or electric trap volume in zone IV. Expected improvements in magnetic traps for ground-state molecules should provide samples of density greater than 10^5 cm^{-3}, as shown by the dotted line in zone IV.

guide. The molecules are slow enough in zone III to be stopped and reflected by an electrostatic [53] or magnetostatic [14] mirror. During the reflection time, the molecules could spend more than a millisecond in the mode of an optimally situated cavity.

Magnetic [14] and electrostatic [54] traps and ac electric traps [55] have been used to trap polar molecules at the terminus of a Stark decelerator, in zone IV. However, room temperature blackbody radiation limits the OH lifetime in these traps to less than 3 s [56]. Thus, the cooling must occur on a time scale much faster than this. While 1 kHz cooling rates, for example, are fast compared to this lifetime, it must be noted that the fraction of the trap volume occupied by the cavity waist can be quite small. Consequently, the molecules do not spend a large amount of time being cooled, and a much larger cooling rate than expected is necessary.

Future work—using numerical cavity cooling simulations incorporating molecular motion—will explore optimal cavity and decelerator geometries for cavity cooling OH. The ground state polar molecular samples are currently 1000 times hotter than the cooling limit imposed by the cavity linewidth. Simulations will address the efficiency and scaling of cooling such hot samples as well. Future improvements to the Stark decelerator technique [52] will produce higher densities of slow molecules, seemingly an important step toward successfully achieving the cavity-assisted laser cooling of molecules. The use of other techniques, such as feedback [57] and optical Stark deceleration [58] may be necessary for increasing the cooling rate and obtaining a larger number of slowed molecules.

In summary, we have identified important necessary conditions for cavity-cooling ground-state molecules, whose open channels and high initial temperatures pose unique challenges. We determine that to prevent Raman loss and thereby achieve efficient cooling, the cooperativity should be greater than unity. Several methods for increasing the coop-

erativity and cooling rate are examined. These include the use of multimode cavities; simultaneously driving (seeding) the cavity mode while transversely pumping the molecular medium; and inducing a self-localizatizing phase transition of the molecules' positions. While multimode cavities are useful for increasing the cavity cooling volume and raising the cooperativity to near unity, only by inducing the superradiant phase transition can one achieve molecular cavity cooling with certainty. We have assessed the feasibility of triggering this superradiant state as well as addressing the possibility of cooling under current experimental constraints, such as uv mirror coating technology, with particular emphasis given to the present performance of OH Stark decelerators. More in-depth numerical simulations of the seeding and self-localization dynamics in the presence of molecule motion—either from a beam or due to a harmonic trap—are required to fully access the feasibility of efficient cavity-assisted laser cooing of molecules. Future work will address these questions via both quantum Monte Carlo simulation [20] and experiment.

ACKNOWLEDGMENTS

APPENDIX A: CAVITY QED OF THREE-LEVEL SYSTEM WITH EXTERNAL PUMP

Solutions to the master equation for the joint molecule-cavity system allow the identification of optimal experimental conditions for achieving cavity-assisted laser cooling. We may investigate multilevel scatters, such as molecules, by bundling all higher states into a single state denoted $|b\rangle$, and assume that the pump laser is so far detuned from the optical transition frequency ω_b that this level can never be depopulated once a single Raman scattering event has occurred (see Fig. 1).

Assuming no coherence develops between the metastable state $|b\rangle$ and either $|a\rangle$ or $|e\rangle$, it is necessary only to include an extra decay term into the standard single-atom cavity QED master equation [30] to properly account for the set of metastable states from which population never returns:

$$\dot{\rho} = -i[\hat{H}, \rho] + \gamma_{\text{Ry}}(2\hat{\sigma}_-\rho\hat{\sigma}_+ - \hat{\sigma}_+\hat{\sigma}_-\rho - \rho\hat{\sigma}_+\hat{\sigma}_-)/2$$
$$- \gamma_{\text{Rn}}[\hat{\sigma}_+\hat{\sigma}_-, \rho]/2 + \kappa(2\hat{a}\rho\hat{a}^\dagger - \hat{a}^\dagger\hat{a}\rho - \rho\hat{a}^\dagger\hat{a}). \quad \text{(A1)}$$

Under the electric dipole and rotating wave approximations, the Hamiltonian describing the coherent dynamics in the presence of both drive and transverse pump fields (whose frequencies are approximately equal) is

$$\hat{H} = -\Delta_{pa}\hat{\sigma}_+\hat{\sigma}_- - \Delta_{pc}\hat{a}^\dagger\hat{a} + g(\hat{a}^\dagger\hat{\sigma}_- + \hat{\sigma}_+\hat{a}) + \Omega_p(\hat{\sigma}_- + \hat{\sigma}_+)/2$$
$$+ \Omega_d(\hat{a} + \hat{a}^\dagger)/2. \quad \text{(A2)}$$

In this equation, $\hat{\sigma}_-$ is the molecular lowering operator, and $\hat{a}$ is the cavity field annihilation operator. The first two terms

are the bare molecule and cavity energies, with $\Delta_{pa} \equiv \omega_p - \omega_a$ and $\Delta_{pc} \equiv \omega_p - \omega_c$, while the molecular pump and cavity drive terms are the fourth and fifth, respectively. The molecule-cavity detuning is $\Delta_{ca} \equiv \Delta_{pc} - \Delta_{pa} = \omega_a - \omega_c$. The cavity energy decay rate is 2κ, and n_c is equal to

$$n_c = \frac{\Omega_d^2/4}{\kappa^2 + \Delta_{pc}^2}. \quad \text{(A3)}$$

All optical fields are far detuned from the molecular resonance in the cavity cooling scenario, and typically $\Delta_{pc} \ll [\Delta_{pa}, \Delta_{ca}]$.

The third term represents the molecule-cavity interaction: excitation is coherently exchanged at the rate g, which depends on the molecule's position in the intracavity mode structure and is inversely proportional to the square root of the cavity mode volume. Specifically, $g = g_0\psi(\hat{r})$ with

$$\hbar g = \vec{\mu} \cdot \vec{\mathcal{E}} = \psi(\hat{r})\mu\sqrt{\frac{\hbar\omega}{2e_0 V_m}} = \psi(\hat{r})\hbar\sqrt{\frac{3c\lambda^2\gamma_\perp}{4\pi V_m}}, \quad \text{(A4)}$$

where $\psi(\hat{r}) \leq 1$ accounts for the molecule's position, $\vec{\mu}$ is the transition dipole moment, and $\vec{\mathcal{E}}$ is the electric field. We have explicitly included Planck's constant in the above equation for clarity, but will set $\hbar = 1$ in all subsequent equations, including Eq. (A2). The mode volume is $V_m \approx \pi w_0^2 L/4$, where w_0 and L are the cavity waist and length, respectively. In the limit that the transition linewidth is dominated solely by radiative processes, $\gamma = 2\gamma_\perp$, where $\gamma_\perp$ is the decay rate of the molecular dipole. In a sense, $2g$ is the Rabi flopping rate of the molecule stimulated by the vacuum field of the cavity.

To obtain the steady-state semiclassical solutions, we make the approximation that all mixed operator expectations are factorable, e.g., $\langle\hat{a}^\dagger\hat{\sigma}_-\rangle \approx \langle\hat{a}^\dagger\rangle\langle\hat{\sigma}_-\rangle$. This allows the separation of Eq. (A1) into two Hamiltonians: one for the molecule, $\hat{H}_a$, in which the cavity operator is converted to a c number $\hat{a} \to \alpha$; and one for the cavity, $\hat{H}_c$, with $\hat{\sigma}_- \to \zeta$, where α is the field amplitude and ζ is the molecular dipole:

$$\hat{H}_a = -\Delta_{pa}\hat{\sigma}_+\hat{\sigma}_- + g(\alpha^*\hat{\sigma}_- + \alpha\hat{\sigma}_+) + \Omega_p(\hat{\sigma}_+ + \hat{\sigma}_-)/2$$
$$= -\Delta_{pa}\hat{\sigma}_+\hat{\sigma}_- + \Omega_p'(\hat{\sigma}_+ + \hat{\sigma}_-)/2, \quad \text{(A5)}$$

$$\hat{H}_c = -\Delta_{pc}\hat{a}^\dagger\hat{a} + g(\zeta\hat{a}^\dagger + \zeta^*\hat{a}) + \Omega_d(\hat{a} + \hat{a}^\dagger)/2$$
$$= -\Delta_{pc}\hat{a}^\dagger\hat{a} + \Omega_d'(\hat{a} + \hat{a}^\dagger)/2. \quad \text{(A6)}$$

The second equalities use the effective molecule drive $\Omega_p' = 2g\alpha + \Omega_p$ and cavity drive $\Omega_d' = 2g\zeta + \Omega_d$ for clarity. The master equation may be similarly separated:

$$\dot{\rho}_a = -i[H_a, \rho_a] + \gamma_\perp(2\hat{\sigma}_-\rho_a\hat{\sigma}_+ - \hat{\sigma}_+\hat{\sigma}_-\rho_a - \rho_a\hat{\sigma}_+\hat{\sigma}_-),$$

$$\dot{\rho}_c = -i[H_c, \rho_c] + \kappa(2\hat{a}\rho_c\hat{a}^\dagger - \hat{a}^\dagger\hat{a}\rho_c - \rho_c\hat{a}^\dagger\hat{a}). \quad \text{(A7)}$$

Setting $\dot{\rho}_a = 0 = \dot{\rho}_c$, we obtain for the steady-state cavity field amplitude

$$\alpha = \text{Tr}(\rho_c\hat{a}) = \frac{\Omega_d'/2}{\Delta_{pc} + i\kappa}, \quad \text{(A8)}$$

and for the molecular coherence

$$\zeta = \text{Tr}(\rho_a \hat{\sigma}_-) = \frac{\Omega_p'/2(\Delta_{pa} - i\gamma_\perp)}{|\Omega_p'|^2/2 + \gamma_\perp^2 + \Delta_{pa}^2}. \tag{A9}$$

From these equations we obtain the molecular excited state population:

$$\sigma_{ee} = \frac{|\Omega_p'/2|^2}{|\Omega_p'|^2/2 + \gamma_\perp^2 + \Delta_{pa}^2}. \tag{A10}$$

To solve the system of Eqs. (A8) and (A9) in closed form, one needs to assume that the molecular excited state is not saturated, i.e., $\gamma_\perp^2 + \Delta_{pa}^2 \gg \Omega_p'^2$. Fortunately, this is exactly the same weak driving condition we must satisfy to prevent the molecule from incoherently scattering.

The saturation parameter s characterizes the boundary between incoherent and coherent scattering:

$$s = \frac{\Omega_p^2/2}{\Delta_{pa}^2 + \gamma^2/4}, \tag{A11}$$

defined here in the absence of a cavity field. Below $s \sim 0.01$, the frequency of coherently scattered photons matches the incoming frequency, and they are emitted in a dipole pattern with respect to the drive beam. In contrast, a saturated molecule scatters photons incoherently into 4π with a linewidth-broadened spectrum. The rate of scattered photons is suppressed in the unsaturated regime, as may be seen from the following relation:

$$\Gamma_a = \frac{\gamma}{2}\frac{s}{(1 + s)} = \gamma\sigma_{ee}. \tag{A12}$$

In the limit that $s \le 1$,

$$\zeta \approx \frac{\Omega_p'/2}{\Delta_{pa} + i\gamma_\perp}, \tag{A13}$$

and the cavity field amplitude becomes

$$\alpha \approx \frac{g\Omega_p/2 + \Omega_d(\Delta_{pa} + i\gamma_\perp)/2}{(\Delta_{pa} + i\gamma_\perp)(\Delta_{pc} + i\kappa) - g^2}. \tag{A14}$$

In the following, we will set the cavity drive to zero, $\Omega_d = 0$, and discuss cavity cooling via transverse pumping solely, as sketched in Fig. 1(c). Energy enters the system only through the pump beam, whose intensity is proportional to Ω_p^2. Energy leaves the system either via the cavity mirrors at a rate proportional to the intracavity field, $\Gamma_c = 2\kappa|\alpha|^2$, or by relaxation of the molecular excited state to modes other than the cavity at rate Γ_a. We assume that the solid angle subtended by the cavity mirrors is much less than 4π. Indeed, for all cavities of interest, the fractional solid angle is $\sim 10^{-5}$, and Γ_a is effectively unmodified by the cavity's presence.

To ensure low molecular saturation, we now apply the dispersive weak driving condition,

$$\Delta_{pa} \gg [\Omega_{pa}, \gamma_\perp, g], \tag{A15}$$

to arrive at the following rate expressions:

$$\Gamma_c \approx 2\kappa\frac{\Omega_p^2}{4\Delta_{pa}^2}\frac{g^2}{\Delta_{pc}^2 + \kappa^2}, \tag{A16}$$

$$\Gamma_a \approx 2\gamma_\perp\frac{\Omega_p^2}{4\Delta_{pa}^2}. \tag{A17}$$

In the previous expressions, we have made the additional assumption that $\Delta_{pa} \gg \Delta_{pc}$, which is true for optimal cooling, which in turn requires $\Delta_{pc} \approx -\kappa$. In light of the previous statement, Eq. (A16) becomes

$$\Gamma_c \approx 2\kappa\frac{\Omega_p^2}{8\Delta_{pa}^2}\frac{g^2}{\kappa^2}, \tag{A18}$$

and the ratio of scattered photons that contribute to cooling to those contributing to heating and Raman loss is

$$C = \frac{\Gamma_c}{\Gamma_a} = \frac{g^2}{2\kappa\gamma_\perp}. \tag{A19}$$

The label C is used to highlight the fact that this enhancement factor is none other than the single-atom cooperativity parameter well known from cavity QED [30]. The cavity field is stimulating the transfer of photons from the pump field to the decaying cavity mode at a rate faster than free-space scattering. The cooperativity may be better understood by noting that the decay rate of the coupled molecule-cavity system, in this limit, is $\Gamma_{ac} \approx \gamma(1 + 2C)\Omega_p^2/\Delta_{pa}^2$. The extra factor $2C$ comes from the increased rate at which the pump field is depleted. It is important to note that the independence of the cavity–to–free-space scattering ratio C on detuning.

When $C < 1$ (weak-coupling limit, assuming $g < [\kappa, \gamma_\perp]$), the cooling process may be described perturbatively as coherent Rayleigh scattering, as was done by Vuletić *et al.* [19,28]. Because previous cavity-cooling literature has used inconsistent and thus confusing terminology, we now provide a remark on language. "Coherent" refers to scattering in the $s \ll 1$ regime, wherein a definite relationship exists between the scattered field and the oscillating molecular dipole. "Rayleigh" refers to the fact that any light scattered into the cavity mode is of a frequency such that the molecule relaxes to the ground state of origin, and is thus an elastic process. This occurs when Δ_{pc} is much smaller than any frequency difference ω_{ab} between $|a\rangle$ and metastable ground states $|b\rangle$. The phrase "coherent Rayleigh" means that the Rayleigh scattering is in a dipole pattern and is of the same frequency and spectral bandwidth as the pump field.

For consistency, we remark that, while the notion of coherence in Raman scattering—which is inherently an inelastic process—is not commonly defined, we take the phrase "coherent Raman scattering" to mean that the character of the scattered field retains a definite relationship to the pump field, which is the case in the $s \ll 1$ regime. While there is a frequency offset between the pump and scattered fields, there is a fixed phase relationship between them, and the field is scattered in a dipole pattern. As discussed extensively in Sec. II, this coherent Raman scattering, which quenches the molecular cooling process, cannot be overcome by making s small. The only remedy is to enhance the molecule-cavity coupling.

Since $g < \kappa$ in this limit, "scattering" is the term of choice because any photon emitted into the cavity escapes via the mirrors before being reabsorbed by the molecule. Thus, the
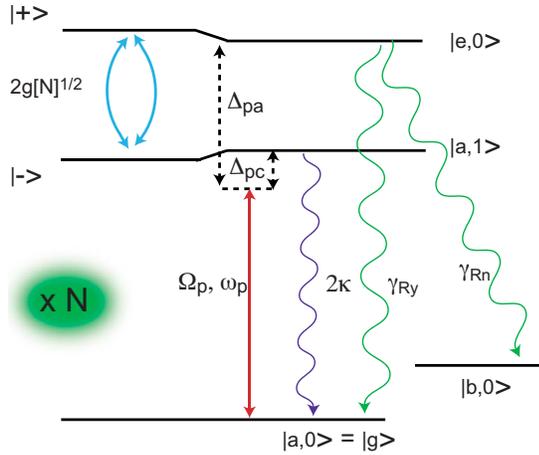
FIG. 5. (Color online) Dressed-state spectroscopy for N three-level atoms (molecules) coupled to a cavity mode in the presence of a transverse pump field Ω_p. The detunings are set to $[\Delta_{pa}, \Delta_{pc}] < 0$ for cavity cooling, and the pump field connects the absolute ground state of the joint system $|g\rangle$ with $|e,0\rangle$. For efficient cavity cooling, the magnitude of Ω_p is set so that the population of $|e,0\rangle$ is low, suppressing both incoherent scattering to $|g\rangle$ and Raman scattering to the secondary ground states, collectively represented by $|b,0\rangle$. With these detunings, the molecule(s)-cavity coupling g mixes the excited states to produce the dressed states $|\pm\rangle$. The lower dressed state $|-\rangle$ may be viewed as a polariton excitation, as it is mostly comprised of the cavity excitation.

cavity field is incidental: the molecule scatters photons from the incoming pump beam to the two beams emanating from the cavity mirrors and the cavity itself serves only to provide a concentrated density of states, which modifies the frequency spectrum of scattered photons. The language of the Purcell effect [61]—enhanced emission into the solid angle subtended by the cavity mirrors—is apt in this situation and Vuletić *et al.* make use of it to describe these dynamics. The Purcell factor is exactly equivalent to the cooperativity, but expressed in a more experimentally recognizable form.

In the good-cavity limit ($[\gamma_\perp, g] > \kappa$) or, more restrictively, the strong-coupling regime ($g > [\kappa, \gamma_\perp]$), the perturbative treatment described above becomes less applicable. This is because an intracavity photon can be reabsorbed coherently by the molecule many times before finally being dissipated via the cavity mirrors or spontaneous emission. The molecule and cavity system can no longer be treated independently and it is advantageous to study the system in the dressed-state picture as shown in Fig. 5. In this figure, the state space of the first excited states of the joint system, $|\pm\rangle$, are being probed by the pump laser of Rabi frequency Ω_p. The addition of the secondary ground state $|b,0\rangle$ accounts for all of the Raman loss channels found in realistic molecules. The inclusion the factor of $\sqrt{N}$ for the N copies of the intracavity particles is discussed in the context of multiparticle effects in Sec. IV. The pump laser can only excite the $|e,0\rangle$ level since the transition to $|a,1\rangle$ is not electric dipole allowed. At low saturations $s \ll 1$, this state decays via coherent elastic Rayleigh scattering γ_{Ry}, to the ground state, which leads to heating. Additionally, inelastic Raman scattering γ_{Rn} may occur, which depopulates $|g\rangle$. The coherent molecule-cavity coupling exchanges population from the molecule's excited state $|e,0\rangle$ to the cavity's excited state $|a,1\rangle$ at the "Rabi" frequency $2g$. Thus, population can be decoupled from molecular decay if $g > \gamma_\perp$, and $|a,1\rangle$ will decay via mirror leakage at the rate 2κ, which leads to cooling.

An alternative, but wholly equivalent, method for deriving Eqs. (A16) and (A17) is to view the pump field as spectroscopically probing the dressed states $|\pm\rangle$, which are found by diagonalizing the Hamiltonian in Eq. (A2). Under the conditions of Eq. (A15), the states are:

$$|+\rangle = c_e|e,0\rangle + c_a|a,1\rangle, \quad (A20)$$

$$|-\rangle = c_a|e,0\rangle - c_e|a,1\rangle, \quad (A21)$$

with

$$|c_e|^2 = 1 - g^2/\Delta_{pa}^2, \quad (A22)$$

$$|c_a|^2 = g^2/\Delta_{pa}^2. \quad (A23)$$

The decay rates and populations of states $|\pm\rangle$ may easily be obtained—with the justifiable assumption that the coherence between them vanishes rapidly—by treating them as independently pumped by Ω_p.

TABLE I. Comparison of the three best OH electronic cooling transitions. $P_1(1)$ has a better bare Rayleigh-to-Raman ratio Υ, but requires one microwave pumping stage and does not have a cycling hyperfine transition. The $Q_1(1)$ transition has a smaller Υ and a cycling transition on $F'' = 1 \rightarrow F' = 2$ if two microwave pumping stages are used to prepare the OH in the $F'' = 1$ hyperfine ground state (see Refs. [25,26] for information regarding state preparation using a microwave cavity at the terminus of a Stark decelerator). A compromise transition is $Q_{21}(1)$, which has an intermediate Υ but no cycling hyperfine transition. Note that the $P_1(1)$ transition is 92% closed with just one repumper on the $P_{12}(1)$ line. Transition wavelengths and lifetimes are from the software packages HITRAN [59] and LIFBASE [60].

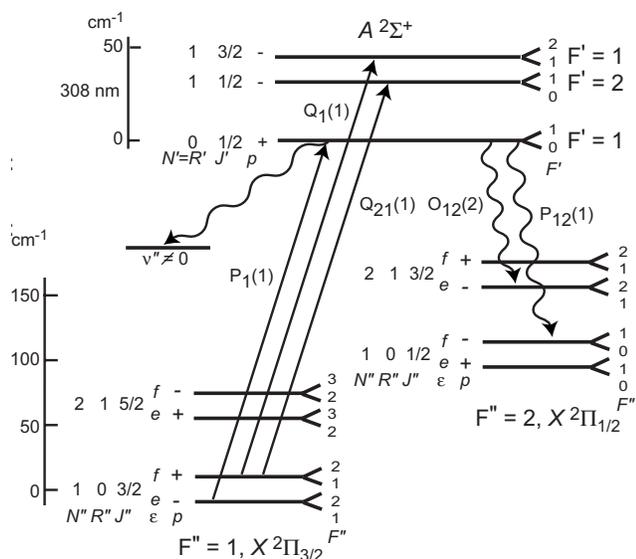|	λ_{ae} (nm)	$[J', N']$	$\Gamma/2\pi$ (10^5 Hz)	Υ	No. of repumpers	$v'' \neq 0$	$\Delta F = +1$?	No. of microwave pulses
$P_1(1)$	308.256	[1/2,0]	2.32	1.43	2	0.4%	No	1
$Q_1(1)$	307.933	[3/2,1]	2.32	0.28	4	4%	Yes	2
$Q_{21}(1)$	307.937	[1/2,1]	2.32	0.65	2	1%	No	0

FIG. 6. OH level diagram depicting the $P_1(1)$, $Q_1(1)$, and $Q_{21}(1)$ electronic transitions. The first excited level A $^2\Sigma^+$ and the two X $^2\Pi$ ground states are shown. For clarity, only the $P_1(1)$ decay channels are shown: $P_{12}(1)$, $O_{12}(2)$, and the $\nu'=0 \rightarrow \nu'' \neq 0$ transitions.

APPENDIX B: CANDIDATE OH COOLING TRANSITIONS

The Stark decelerator provides samples of weak-field-seeking $F''=1$, X $^2\Pi_{3/2}$ OH molecules [12]. $F''=1$ is spectroscopic notation for the lower-energy state of a doublet ($F=1$, $J=N+1/2$, while for $F=2$, $J=N-1/2$) and is not the hyperfine quantum number F, which is italicized. The double prime denotes ground-state quantum numbers, while a single prime refers to the excited state. The total angular momentum is equal to $\vec{J}=\vec{L}+\vec{S}+\vec{R}$, where the three vectors are orbital, spin, and rotational angular momentum, respectively. The angular momentum N is defined as $\vec{N}=\vec{R}+\vec{L}$.

The majority of the OH ground-state population arrives at the terminus of the decelerator in the $\nu''=0$, $F''=2$, $\epsilon=f$ symmetry, and $p=+$ parity state. Microwaves can easily transfer this population to the $e,-$ lower Λ-doublet states [25,26]. The total angular momentum in the $F''=1$, X $^2\Pi_{3/2}$ ground state is $J''=3/2$. The orbital plus rotational angular momentum quantum number in this ground state is $N''=R''+L''=1$.

Electric dipole transitions are allowed between transitions of opposite parity that satisfy $\Delta J=0, \pm1$, and $\Delta N=0, \pm1, \pm2$, where $\Delta J=J'-J''$ and $\Delta N=N'-N''$. The strongest electronic cooling transitions that originate in the $F''=1$, X $^2\Pi_{3/2}$ ground state are $P_1(1)$, $Q_1(1)$, and $Q_{21}(1)$. The spectroscopic notation is defined as [62] $\Delta N_{F'F''}(N'')$, where $\Delta N\equiv[-2,-1,0,1,2]\rightarrow[O,P,Q,R,S]$. In this notation, if $F'=F''$, then only one subscript index is used.

Table I lists the properties of the $^2\Pi_{3/2}$ to $^2\Sigma^+_{1/2}$ ($\Delta\nu=0$ band) transitions of interest. To cool on the $P_1(1)$ transition, a single microwave pulse is needed to drive the population to the e state. The other two electronic transitions need either one additional microwave pulse [$Q_1(1)$] or no microwaves at all [$Q_{21}(1)$] for initial state preparation. Only $Q_1(1)$ offers the possibility of a $\Delta F=+1$ transition, which allows the molecule to easily return to the same Zeeman hyperfine ground state after each Rayleigh scattered photon. The recoil frequency for these transitions is: $\omega_{\mathrm{rec}}=2\pi\times1.23\times10^5$ Hz.

With two repumpers, one each on the $P_{12}(1)$ and the $O_{12}(2)$ lines, the $P_1(1)$ transition remains 0.4% open due to the possibility of scattering to higher vibrational levels (i.e., $\nu'' \neq 0$). Closing the $Q_1(1)$ transition to 4% requires—in order of importance—repumpers on the $P_{12}(1)$, $Q_{12}(1)$, $P_1(2)$, and $Q_{12}(3)$ lines. To close the $Q_{21}(1)$ transition to 1% requires repumping the $Q_2(1)$ and $P_2(2)$ lines. Figure 6 sketches the relevant energy levels for the electronic transitions, but for clarity only includes the decay channels from the $P_1(1)$ transition. The first vibrational transition, $Q_{\frac{3}{2}}e$, may be completely closed with five repumpers and is ~60% closed with just one repumper on the $P_{\frac{5}{2}}f$ line, where the notation is $\Delta J(J'')\epsilon$ and $\epsilon=e,f$.

[1] J. Doyle, B. Friedrich, R. Krems, and F. Masnou-Seeuws, Eur. Phys. J. D **31**, 149 (2004).

[2] A. V. Avdeenkov and J. L. Bohn, Phys. Rev. Lett. **90**, 043006 (2003).

[3] C. Ticknor and J. L. Bohn, Phys. Rev. A **71**, 022709 (2005).

[4] R. V. Krems, Int. Rev. Phys. Chem. **24**, 99 (2005).

[5] E. R. Hudson, C. Ticknor, B. C. Sawyer, C. A. Taatjes, H. J. Lewandowski, J. R. Bochinski, J. L. Bohn, and J. Ye, Phys. Rev. A **73**, 063404 (2006).

[6] D. DeMille, Phys. Rev. Lett. **88**, 067901 (2002).

[7] A. Micheli, G. Brennen, and P. Zoller, Nat. Phys. **2**, 341 (2006).

[8] J. M. Sage, S. Sainis, T. Bergeman, and D. DeMille, Phys. Rev. Lett. **94**, 203001 (2005).

[9] D. Wang *et al.*, Eur. Phys. J. D **31**, 165 (2004).

[10] J. Weinstein, R. deCarvalho, T. Guillet, B. Friedrich, and J. Doyle, Nature (London) **395**, 921 (1998).

[11] H. L. Bethlem, G. Berden, and G. Meijer, Phys. Rev. Lett. **83**, 1558 (1999).

[12] J. R. Bochinski, E. R. Hudson, H. J. Lewandowski, G. Meijer, and J. Ye, Phys. Rev. Lett. **91**, 243001 (2003).

[13] S. Y. T. van de Meerakker, P. H. M. Smeets, N. Vanhaecke, R. T. Jongma, and G. Meijer, Phys. Rev. Lett. **94**, 023004 (2005).

[14] B. C. Sawyer, B. L. Lev, E. R. Hudson, B. K. Stuhl, M. Lara, J. L. Bohn, and J. Ye, Phys. Rev. Lett. **98**, 253002 (2007).

[15] H. J. Metcalf and P. van der Straten, *Laser Cooling and Trapping* (Springer-Verlag, New York, 1999).

[16] J. Bahns, W. C. Stwalley, and P. Gould, J. Chem. Phys. **104**, 9689 (1996).

[17] M. D. Rosa, Eur. Phys. J. D **31**, 395 (2004).

[18] M. Lara, J. L. Bohn, D. Potter, P. Soldán, and J. M. Hutson, Phys. Rev. Lett. **97**, 183201 (2006).

[19] V. Vuletić and S. Chu, Phys. Rev. Lett. **84**, 3787 (2000).

[20] P. Domokos and H. Ritsch, J. Opt. Soc. Am. B **20**, 1098

(2003).

[21] W. Lu, Y. Zhao, and P. F. Barker, Phys. Rev. A **76**, 013417 (2007).

[22] G. Morigi, P. W. H. Pinske, M. Kowalewski, and R. de Vivie-Riedle, Phys. Rev. Lett. **99**, 073001 (2007).

[23] A. V. Avdeenkov and J. L. Bohn, Phys. Rev. A **66**, 052718 (2002).

[24] J. J. Gilijamse, S. Hoekstra, S. van de Meerakker, G. Groenenboom, and G. Meijer, Science **313**, 1617 (2006).

[25] E. R. Hudson, H. J. Lewandowski, B. C. Sawyer, and J. Ye, Phys. Rev. Lett. **96**, 143004 (2006).

[26] B. L. Lev, E. R. Meyer, E. R. Hudson, B. C. Sawyer, J. L. Bohn, and J. Ye, Phys. Rev. A **74**, 061402(R) (2006).

[27] P. Horak, G. Hechenblaikner, K. M. Gheri, H. Stecher, and H. Ritsch, Phys. Rev. Lett. **79**, 4974 (1997).

[28] V. Vuletić, H. W. Chan, and A. T. Black, Phys. Rev. A **64**, 033405 (2001).

[29] P. Domokos, T. Salzburger, and H. Ritsch, Phys. Rev. A **66**, 043406 (2002).

[30] H. J. Kimble, *Cavity Quantum Electrodynamics* (Academic Press, San Diego, 1994).

[31] H. Mabuchi and A. C. Doherty, Science **298**, 1372 (2002).

[32] H. W. Chan, A. T. Black, and V. Vuletić, Phys. Rev. Lett. **90**, 063003 (2003).

[33] A. T. Black, H. W. Chan, and V. Vuletić, Phys. Rev. Lett. **91**, 203001 (2003).

[34] S. Nussmann, K. Murr, M. Hijlkema, B. Weber, A. Kuhn, and G. Rempe, Nat. Phys. **1**, 122 (2005).

[35] K. Murr, Phys. Rev. Lett. **96**, 253001 (2006).

[36] K. Murr, P. Maunz, P. W. H. Pinkse, T. Puppe, I. Schuster, D. Vitali, and G. Rempe, Phys. Rev. A **74**, 043412 (2006).

[37] K. Murr, S. Nuszmann, T. Puppe, M. Hijlkema, B. Weber, S. C. Webster, A. Kuhn, and G. Rempe, Phys. Rev. A **73**, 063415 (2006).

[38] *Atom-Photon Interactions*, edited by C. Cohen-Tannoudji, J. Dupont-Roc, and G. Grynberg (John Wiley and Sons, New York, 1998).

[39] A. Vukics, P. Domokos, and H. Ritsch, J. Opt. B: Quantum Semiclassical Opt. **6**, 143 (2004).

[40] S. Y. T. van de Meerakker, N. Vanhaecke, M. P. J. van der Loo, G. C. Groenenboom, and G. Meijer, Phys. Rev. Lett. **95**, 013003 (2005).

[41] D. J. Heinzen and M. S. Feld, Phys. Rev. Lett. **59**, 2623 (1987).

[42] A. E. Siegman, *Lasers* (University Science Books, Sausalito, CA, 1986).

[43] H. Chan, Ph.D thesis, Stanford University, 2003.

[44] P. Domokos and H. Ritsch, Phys. Rev. Lett. **89**, 253003 (2002).

[45] J. K. Asbóth, P. Domokos, H. Ritsch, and A. Vukics, Phys. Rev. A **72**, 053417 (2005).

[46] R. H. Dicke, Phys. Rev. **93**, 99 (1954).

[47] Y. Kaluzny, P. Goy, M. Gross, J. M. Raimond, and S. Haroche, Phys. Rev. Lett. **51**, 1175 (1983).

[48] S. Zippilli, G. Morigi, and H. Ritsch, Phys. Rev. Lett. **93**, 123002 (2004).

[49] A. Black, H. Chan, and V. Vuletić, in *Proceedings of the 16th International Conference on Laser Spectroscopy (ICOLS 2003, Palm Cove)*, edited by P. Hannaford, A. Sidorov, H. Bachor, and K. Baldwin (World Scientific, Singapore, 2004), p. 345.

[50] P. R. Berman, Phys. Rev. A **59**, 585 (1999).

[51] E. R. Hudson *et al.*, Eur. Phys. J. D **31**, 351 (2004).

[52] B. C. Sawyer, B. K. Stuhl, B. L. Lev, J. Ye, and E. R. Hudson, (unpublished).

[53] S. A. Schulz, H. L. Bethlem, J. van Veldhoven, J. Küpper, H. Conrad, and G. Meijer, Phys. Rev. Lett. **93**, 020406 (2004).

[54] S. Y. T. van de Meerakker, P. H. M. Smeets, N. Vanhaecke, R. T. Jongma, and G. Meijer, Phys. Rev. Lett. **94**, 023004 (2005).

[55] J. van Veldhoven, H. L. Bethlem, and G. Meijer, Phys. Rev. Lett. **94**, 083001 (2005).

[56] S. Hoekstra, J. J. Gilijamse, B. Sartakov, N. Vanhaecke, L. Scharfenberg, S. van de Meerakker, and G. Meijer, Science **313**, 101 (2006).

[57] W. Lu and P. F. Barker, Phys. Rev. A **72**, 025402 (2005).

[58] R. Fulton, A. Bishop, M. Shneider, and P. Barker, Nat. Phys. **2**, 465 (2006).

[59] L. Rothman *et al.*, J. Quant. Spectrosc. Radiat. Transf. **96**, 139 (2005).

[60] J. Luque, computer code LIFBASE 2.0, SRI International (2005).

[61] E. Purcell, Phys. Rev. **69**, 37 (1946).

[62] G. H. Dieke and H. M. Crosswhite, J. Quant. Spectrosc. Radiat. Transf. **2**, 97 (1962).